# UNCLASSIFIED

## AD 415742

DEFENSE DOCUMENTATION CENTER

FOR

SCIENTIFIC AND TECHNICAL INFORMATION

CAMERON STATION, ALEXANDRIA, VIRGINIA

# UNCLASSIFIED

# SEVENTH
# QUARTERLY PROGRESS
# REPORT

PREPARED UNDER
U. S. ARMY SIGNAL CORPS CONTRACT
DA-36-039-SC-87318

UNDER Γ..IE TECHNICAL SUPERVISION
OF THE ATOMICS BRANCH OF
THE APPLIED PHYSICS DIVISION
U. S. ARMY SIGNA! RESEARCH AND
DEVELOPMENT LABORATORIES
AT FORT MONMOUTH

by

M. N. HIRSH
P. N. EISNER

R-146-7                                    31 MARCH 1963

## THE G. C. DEWEY CORPORATION

AN EXPERIMENTAL INVESTIGATION OF
THE EFFECTS OF RADIATION ON THE PROPOGATION
OF ELECTROMAGNETIC SIGNALS IN AIR

SEVENTH QUARTERLY PROGRESS REPORT

Prepared under
U. S. Army Signal Corps Contract
DA-36-039-SC-87318

Under the Technical Supervision
of The Atomics Branch of
The Applied Physics Division
U. S. Army Signal Research and
Development Laboratories
at Fort Monmouth

Report R-146-7

by

M. N. Hirsh
P. N. Eisner

31 March 1963

THE G. C. DEWEY CORPORATION
202 East 44th Street
New York 17, New York

## TABLE OF CONTENTS

## I.  INTRODUCTION

The present report covers work performed during the period 1 January to 31 March 1963.  It begins with a description of modifications made to the experimental equipment to permit the measurement of time-dependent ionization phenomena.  The results of transient measurements in oxygen and $N_2 - O_2$ mixtures using these techniques is then presented.  A detailed calculation of the role of diffusion in transient ionization phenomena has been started and is discussed in the report.  The report closes with a description of the proposed work for the next quarter.

During the period covered by the report, the authors delivered a paper at the New York meeting of the American Physical Society,[1] in which the techniques of the present program, together with preliminary data on oxygen loss processes, were discussed.

(1)  M. N. Hirsh and P. N. Eisner, Bull Am. Phys. Soc. II, vol. 8, p. 58 (1963)

## II. EXPERIMENTAL EQUIPMENT

### A. RF Circuit

In Section III, a series of transient experiments will bo
described which utilize the electron beam switch described in
previous reports. However the rf system described in previous
reports has been arranged to give measurements in the steady
state only. For these experiments the measuring circuits were
modified through the use of timing and triggering circuits to
enable rf measurements to be made as a function of time after the
electron beam turn-on.

A block diagram of this system is shown in Figure 1; the
timing sequence of this system is shown in Figure 2. All operations
within this system are periodic, with a cyclic rate determined by
the sweep frequency of a tektronix Model 545 oscilloscope, whose
sawtooth output triggers the Van de Graaff's electron beam switch
through the relay circuit explained in the Sixth Quarterly Report.
The oscilloscope also has an adjustable delayed sweep. The trigger
from this delayed sweep initiates the sweep of another sawtooth
generator; the output of which is used in two ways, first to drive
the external sweep mechanism of the read-out scope, a type 5G2,
Tektronix Dual-Beam Oscilloscope and second, to sweep the frequency
of the 0-5 mcps oscillator used as the modulation oscillator in the
rf bridge.

In Figure 2, Trace 3 represents the sawtooth which sweeps the
frequency of the modulation oscillator. When this oscillator is at
the correct frequency for cavity resonanace, a pip will be seen on
channel A of the dual beam scope. This is shown in Figure 2 on
Trace 4. The time at which this occurs is determined by reading
time $T_3 - T_2$ from the trace on channel A of the dual beam scope
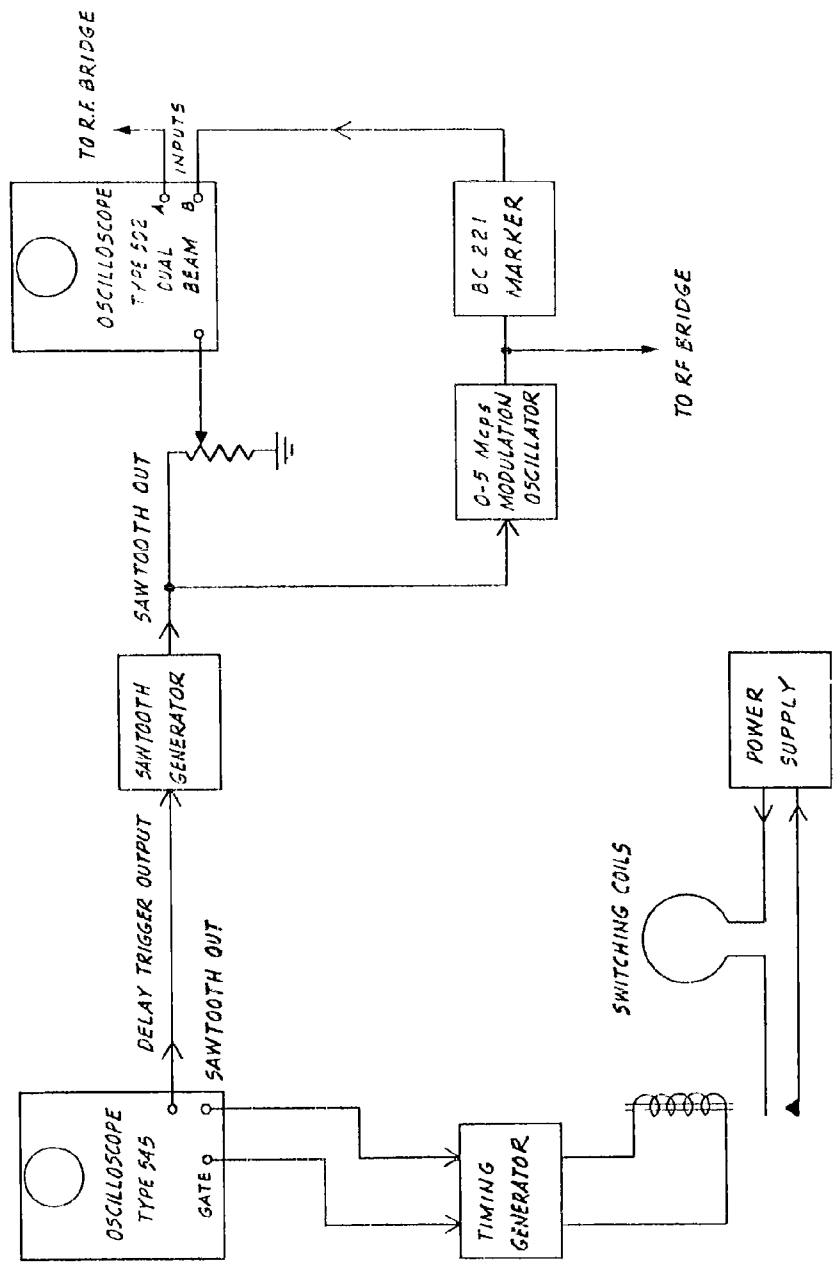
FIGURE 1

BLOCK DIAGRAM OF TIMING CIRCUITS FOR
TRANSIENT MEASUREMENTS

4
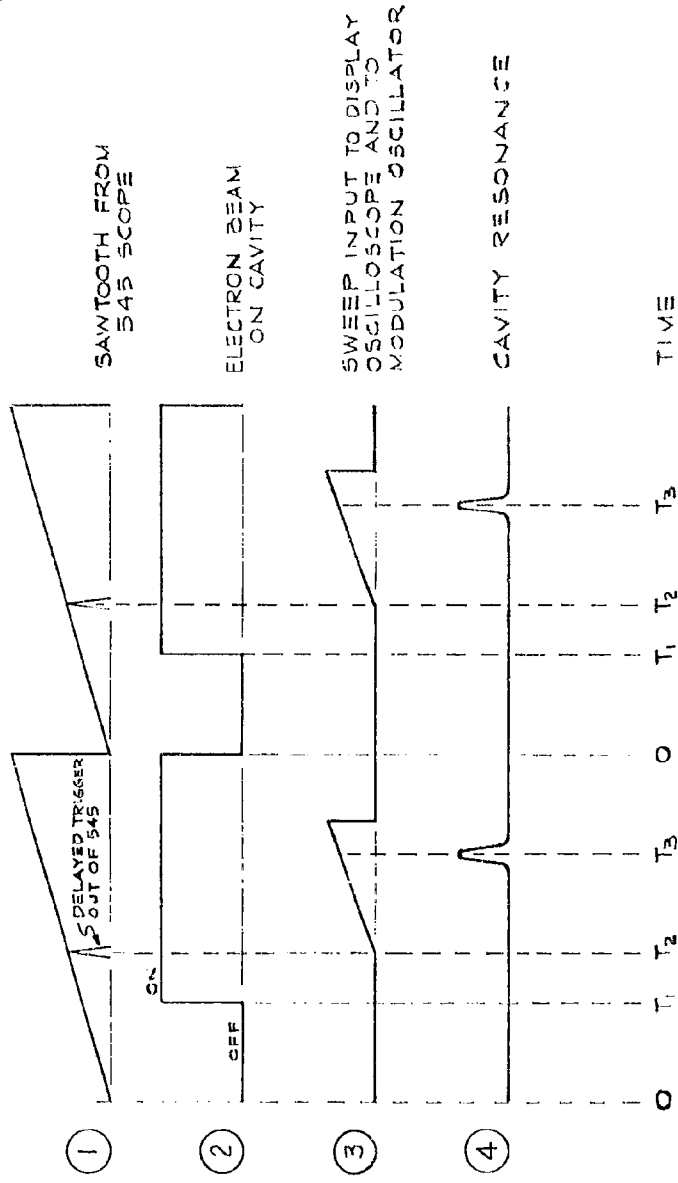


FIGURE 2
TIMING SEQUENCE FOR TRANSIENT MEASUREMENTS

and adding to that the delayed trigger time $T_2$. Time $T_1$ can be determined by moving the delayed trigger until the turn-on of the electron beam is observed.

The system described above has a time resolution capability of about one millisecond which is adequate for timing the transients which have been observed so far. The accuracy and time resolution is mainly determined by the stability and speed of the electron-beam switching mechanism which is a relay actuated device. Improvements could be made by using an all-electronic switch and coils of lower inductance to switch the beam faster.

B.  Foil Diffuser

On page 4 of the Fifth Quarterly Report it was reported that "further work on the beam diffusion problem was deferred until after the air and oxygen experiments were completed so that any information learned from these experiments could be incorporated into the next equipment changes." That time has now come.

Several important points have been learned from the results of the steady-state experiments, which have a bearing on the primary electron diffusion. First, the net ionization observed at low pressures in oxygen cannot be related to fundamental mode ambipolar diffusion if a homogeneous distribution of primary electrons is assumed. This point will be explained in Section IV. Second, at high pressures in oxygen where ionization measurements point to a three body electron attachment as the dominant electron removal process, the numerical value of that coefficient depends on the net primary (high energy) electron current traversing the microwave cavity. Since direct attempts to measure this current failed (cf Sixth Quarterly Report), assumptions concerning the angular distribution of scattering in beryllium foils must be made in order to calculate the percentage of the beam which enters the cavity.

6

However, these assumptions, which will be explained in this
section, do not lead to the accepted value for the three body
attachment coefficient. The third point to be considered is an
experiment described in the Fifth Quarterly Report which indicated
that even with .024 inches of beryllium foil, the electron beam
only covered an area corresponding to a diameter of 2 to 3 feet at
the cavity face. The cavity face has a diameter of 4 feet, so that
there is not a homogeneous distribution of electrons across its face.
Thus during this quarter measurements were made of the beam current
passing through the foil and collimator in order to determine the
electron beam disbribution and the actual percentage of the beam
transmitted by the foil and collimator. Figure 3 schematically
illustrates the method used.

A - SWITCHING COILS
B - FOIL DIFFUSER
C - COLLIMATOR
D - INSULATING FLANGE
E - FARADAY CUPS
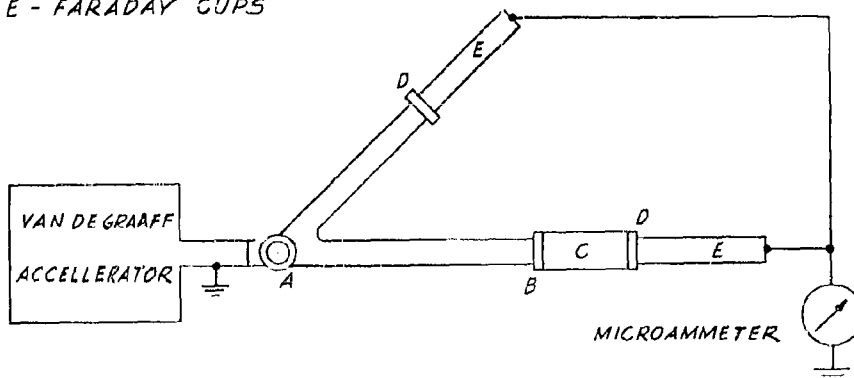


FIGURE 3
FOIL SCATTERING CALIBRATION TECHNIQUE

A section of 2" diameter beam tube between the Van de Graaff and
the beam switching section was removed, leaving room for a long
faraday cup after the collimator. The electron beam is alternately
switched between the two faraday cups. Immediately it was dis-
covered that much more current was collected in the faraday cup
behind the collimator than a calculation based upon this test
geometry indicated was possible. It was believed that this was
either due to poor collimation following the scattering foil or
to porous beryllium foil, resulting in under estimation of the
scattering angle. Titanium foil 1.2+.05 mils thick was substituted
for the beryllium. This foil also appeared to scatter the electrons
less than the calculated amount. The density of the titanium foil
was measured, and found to be 4.5 $gm/_{cm}{}^3$, in excellent agreement
with published values; this value was used in the scattering cal-
culation itself. Therefore poor electron collimation due to
glancing of electrons off the walls of the collimator was the
probable fault. A new collimator was designed and tested which
eliminated this problem. With the new collimator, 21.8% of the
beam was collected in the faraday cup; this compares with a cal-
culated percentage for this geometry of 21.2% for Titanium foil
1.2 x $10^{-3}$ inches thick. However, the five beryllium foils used
in previous experiments transmitted 58.5% with the new collimator,
as compared with the calculated transmission for the .024" thickness
of 44.8%. This discrepancy still remains unexplained. Nevertheless,
a beam current calibration for the foils was obtained. For a
gaussian angular scattering distribution, the titanium foil will
produce a distribution of primary electron across the cavity face
uniform to within 5% in flux.

The calculation of the foil scattering distribution proceeds
as follows. The mean scattering angle as a function of electron
energy E and the composition of the scattering foil is[*]

[*] D. M. Ritson, Techniques of High Energy Physics, pg. 9, Interscience,
N. Y. (1961)

$$(1) \quad \langle \theta^2 \rangle \simeq \left( \frac{21}{E} \right)^2 \, X,$$

where X is the distance in units of radiation length. For Be, X is $67 \text{gm/cm}^2$; for titanium it is $16.6 \text{gm/cm}^2$. These have been calculated from

$$(2) \quad \frac{1}{X_o} = 1.37 \times 10^{-3} \, \frac{Z(Z+1)}{A} \, \log_e \, \frac{183}{\sqrt[3]{Z}} \quad \text{gm/cm}^2.$$

If the Gaussian scattering assumption is correct, then the standard deviation $\sigma = \sqrt{\frac{\langle \theta^2 \rangle}{2}}$. The percentage of the beam transmitted in a given angle can then be found from tables of the normal distribution.

C.  Gas Handling System

In the past quarter, the gas handling system was modified to include 12 one-liter flasks. These were used up during this quarterly report period and were replaced by 100-liter cylinders of research grade oxygen and nitrogen. This is nominally the same purity gas as contained in the glass flasks but the gas has not been mass analyzed. One liter of gas at atmospheric pressure fills the cavity to a pressure of 1 Torr; in order to experiment at higher pressures conveniently the quantity of gas available had to be increased beyond the capacity of the one-liter flasks.

Bakeable pyrex Hastings vacuum gauges were inserted directly into the glass portion of the gas handling system (Figure 4). One gauge measures pressure in the range 0-100 microns; the other is used in the range 0-20 Torr. These gauges are calibrated for air and must therefore be calibrated against an absolute gauge for other gases or mixtures. However once this calibration has been done these gauges allow gas pressure measurements without the possibility of contaminating the sample gas in the cavity.

Neither the gas flow regulators nor the metal-to-glass seals in this system are bakeable, therefore this gas handling system is an interim design to permit high pressure measurements in the cavity. At the same time it will be learned whether the gas in the metal cylinders gives the same results as that in the glass flasks, so that a bakeable system can be built around the 100-liter cylinders in the future.
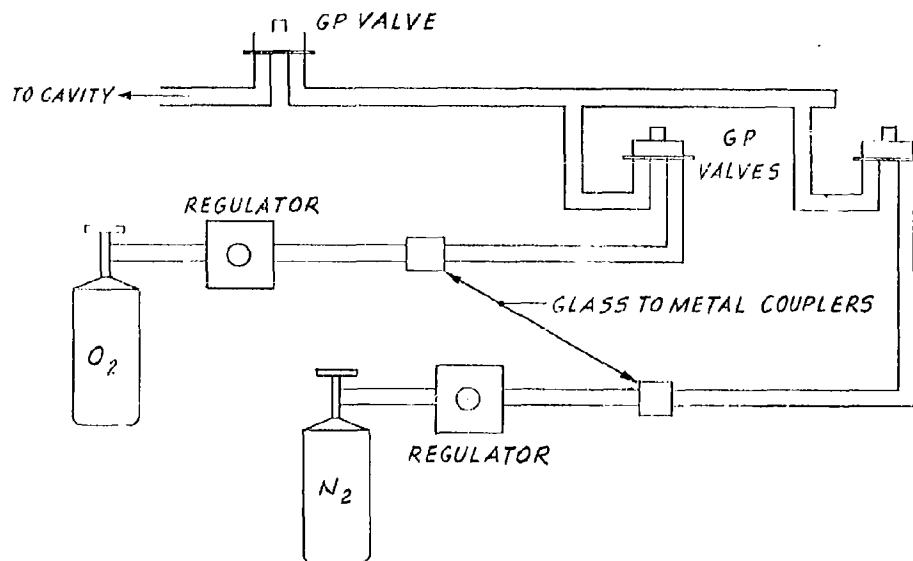


FIGURE 4
GAS HANDLING SYSTEM

### III.   TRANSIENT MEASUREMENTS IN OXYGEN

#### A.   Photographic Technique

Transient measurements were made in oxygen, which were designed
to observe the onset of diffusion in an effort to explain the be-
havior of the low pressure, diffusion dominated, steady-state ion-
ization.   These experiments used the Be foil diffuser.   The technique
used was to tune the rf oscillator to the cavity resonant frequency
and then switch the electron beam onto the cavity.   The result was
that, as the cavity shifted frequency due to the presence of free
electrons, the output signal from the bridge as observed on the
oscilloscope would change as shown in Figure 5.

CAVITY RESONANCE

SCOPE DISPLAY

A B
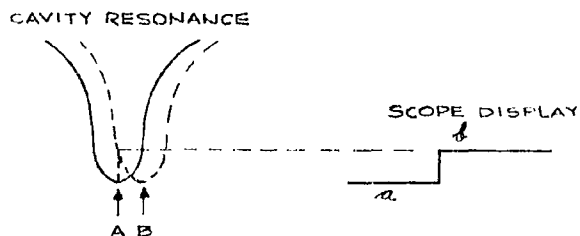
FIGURE 5

During the time when there is no electron beam in the cavity, the
cavity resonance frequency is at A, yielding a straight line at
amplitude "a" on the scope.   The electron beam causes a frequency
shift of the cavity from A to B which changes the observed amplitude
on the scope from "a" to "b", because the oscillator frequency remains
at A.   Figure 6 is a reproduction of a photograph taken of the
oscilloscope face during the turn-on of the electron beam.   The
important feature of these data is the rapid change in frequency
immediately after the turn-on, followed by a slow change in the

12

opposite direction. The beam remains on the cavity during this
experiment, so that a final frequency shift corresponding to the
equilibrium value of ionization is seen, which is the same frequency
measured in steady-state experiments. A reasonable interpretation
of the phenomenon described above is that the slow shift in cavity
frequency to an equilibirum value is due to diffusion of electrons
and ions to the walls of the cavity until the diffusion process
(which is the slowest loss process in the cavity) comes to equilibrium.
Accordingly this transient phenomona was observed photographically
for three pressures of oxygen, 0.11 Torr, 0.07 Torr, and 0.035 Torr.
The decay of the slow transient was found to be an exponential
function of time; the decay time was a linear function of pressure:

$$\tau \text{ (Seconds)} = 1.9 \times 10^3 p \text{ (Torr)}.$$

This yields a constant $D_a p = 120 \text{ Torr-cm}^2/\text{sec}$ assuming the decay
is due to ambipolar diffusion proceeding in the fundamental mode.

However, a $D_a p$ of 120 does not explain the low values of
equilibrium ionization observed in both the steady-state experiments
and in the transient experiments. This point was made before in the
Sixth Quarterly report with respect to the steady-state experiments.
The possible reasons for the discrepancy in numbers between an
apparent measurement of the diffusion decay time, and the diffusion
decay time required to produce the measured equilibrium ionization
will be discussed in Section IV.

Photographs were also taken of the shut-off of the electron
beam which showed a decay time similar to the rise time at

the beam turn-on (see Figure 6). The time constants involved are
on the order of a few milliseconds but were very difficult to
measure accurately with this technique. The time constant associated
with the shut-off is of great importance, however, since it gives
directly a value for the total electron loss frequency. This can
then be compared with the value calculated from the steady state
data by

Kpi = $\gamma_L N$, where K is the production term and $\gamma_L$ is the loss
frequency.

B. Electronic Technique

The photographic work described above was difficult to interpret
quantitatively. Thus measurements were made on transient phenomona
in oxygen using the new rf system described in Section IIA and using
the titanium foil diffuser. From Figure 6 with the assumption of an
exponential decay of frequency versus time,

(1) $f = (f_o - f_1)e^{-t/\tau} + f_1$, or

(2) $\Delta f = f - f_1 = (f_o - f_1)e^{-t/\tau}$.

Taking logarithms of both sides,

(3) $\log \Delta f = \log(f_o - f_1) - t/\tau$

Figure 7 is a plot of the slow (diffusion) transient in oxygen at
0.1 Torr using the time resolving rf circuits which shows reasonable
agreement with the straight line predicted by equation (3). As
indicated in Figure 7, the straight line fit to the data yields a
calculated value of 101 Torr-cm$^2$/sec for $D_a p$ in agreement with
estimates from the photographs. At a pressure of .05Torr, the
measured $D_a p$ was 66.3 Torr-cm$^2$/sec which is not in agreement with
theory or the earlier photographic measurements.

14



OXYGEN 0.11 TORR
7.5 μa ELECTRONBEAM
MEASURED AT FARADAY CUP
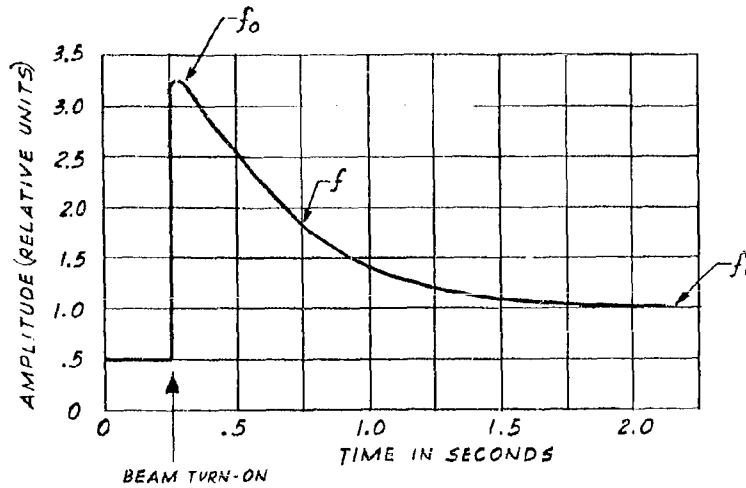
FIGURE 6
TRANSIENT WAVE SHAPE OBTAINED
PHOTOGRAPHICALLY

Figure 7

APPROACH TO STEADY STATE IONIZATION

$O_2$ AT 0.1 TORR

$\mathcal{T} = 228$ MILLISECONDS

$D_a P = .101$

MILLISECONDS

$\Delta f$ IN BC 231 UNITS

16
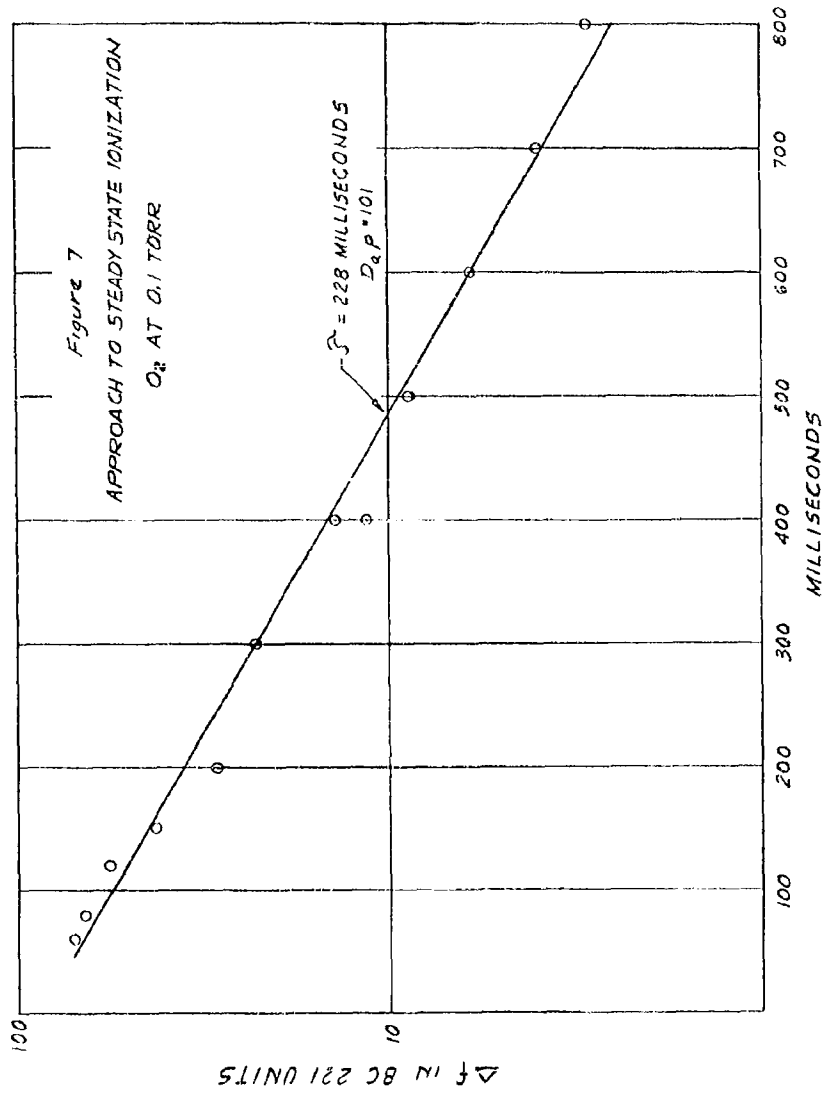
A summary of oxygen transient measurements is presented below:

| Date | Pressure Torr | Beam Current Faraday cup | $\Delta f/I$ Equilibrium Slope | $n_a p$ |
|------|------|------|------|------|
| March 15 | 0.102 | 97.8 ua | 0.78 | 105 |
| March 18 | 0.010 | 150 ua | ? | ? |
| March 19 | 0.050 | 30 ua | 0.27 | 66.3 |
| March 25 | 0.100 | 50 ua | 0.68 | 101 |
| March 28 | 0.102 | 150 ua | 0.76 | ? |

The beam current was measured at the faraday cup in the upper arm
of the beam switch; a titanium foil 1.2 mils thick was used
to diffuse the beam into the cavity (see Section II-B). The
question marks indicate that a measurement could not be made due
to experimental difficulties or malfunction.

C.  Summary of Results of Oxygen Experiments

Previous measurements of equilibrium ionization in oxygen at
0.1 Torr pressure resulted in a "slope", $\Delta f/I$ of 1.7 $Kcps/\mu a$
(c.f. Sixth Quarterly Report). These measurements were made using
a beryllium foil 0.024 inches thick. The foil measurements made
during this quarter predict that 58.5% of the electron beam was
intercepted at the cavity. Therefore the slope, corrected for the
actual beam current in the cavity, is 2.9 kilocycles per micro-
ampere. The experiments of this quarter with a 0.0012 inch thick
titanium foil yielded a true slope, at 0.1 Torr, of 3.52 kilocycles
per microamperes, certainly larger than previous results. However
the beam geometry in the two cases is different; with the beryllium
foil the beam was peaked in the center whereas with the titanium
foil a uniform beam was achieved. The effect of the uniformity of
the beam will be explained in Section IV.

Since the steady-state ionization equation has been derived
on the assumption of geometically uniform production of electron-
ion pairs by the high energy electron beam, the experiments using
the beryllium foil could not be expected to agree with the simple
theory as put forth in the Sixth Quarterly report, Section III-A.
Not enough data has been taken yet with the thin titanium foil to
compare with previous results or with the more complete theory
presented in Section IV of this report.

The various transient experiments have produced evidence for
diffusion of electrons to the walls following turn-on of the high
energy electron beam. The time constants involved are of the same
order of magnitude as those of fundamental mode ambipolar diffusion
in oxygen. Furthermore there is some evidence that the product of
the time constant and pressure is a constant, as required for
diffusion, although much more data still are required.

In order to make sure that the transient phenomena were not
unique to the oxygen gas sample used, the cavity was filled with
cylinder helium to a pressure of 0.08 Torr. A transient similar
to the oxygen transient was observed. In air, the same type of
transient has also been observed.

## IV. DIFFUSION

### A. Time-Dependent Diffusion Equation for An Attaching Gas

The attempt to relate the transient phenomona reported above with ambipolar diffusion makes necessary a careful analysis of ionization and deionization within the cavity. In particular, the time dependence of the ionization density as a function of position within the cavity must be included in the analysis. Such calculations have been performed in the past by many workers, with little opportunity for comparison of the calculation with experimental results. The simplicity of the geometry of the present experiment, however, holds out hope for something approaching a clear-cut determination of the importance of higher diffusion modes in thermal plasmas.

The differential equation for electron density is

$$(1) \quad \frac{n(r,z,t)}{t} \quad = \quad K(r,z,t) - \nu n(r,z,t) + D_a \nabla^2 n(r,z,t),$$

where n is the electron density, K is the number of electrons (and ions) produced per unit volume per unit time, $\nu$ is the three-body attachment frequency, and $D_a$ is the ambipolar diffusion constant (c.f. First Quarterly Progress Report, pages 9-12).

The simplifying assumptions on which the derivation of this equation is based are that the presence of negative ions due to attachment does not affect the ambipolar diffusion; that there is cylindrical symmetry; that other electron loss processes are small compared to three-body attachment and diffusion; and that there are no chemical reactions taking place in the cavity. The first of these assumptions will be the subject of future work in this project.

20

The homogeneous part of equation (1) can be separated and solved subject to the usual boundary condition that n vanish at the walls of the cylindrical cavity. The homogeneous solution is

$$(2) \quad n_H = \sum_n \sum_m A_{nm} J_o (\gamma_n \frac{r}{a}) \sin \frac{m\pi z}{h} e^{-\beta_{nm} t},$$

where $\gamma_n$ is the nth root of $J_o$, a and h are the radius and height of the cylindrical cavity, respectively,

$$(3) \quad \beta_{nm} = \nu + \frac{D_a}{\Lambda^2_{nm}}, \text{ and}$$

$$(4) \quad \frac{1}{\Lambda^2_{nm}} = \frac{\gamma^2_n}{a^2} + \frac{m^2 \pi^2}{h^2}.$$

The inhomogeneous solution which satisfies the complete equation and the initial conditions is

$$(5) \quad n_I = \sum_n \sum_m B_{nm} J_o (\gamma_n \frac{r}{a}) \sin \frac{m\pi z}{h}, \text{ where}$$

$$(6) \quad K = \sum_n \sum_m \beta_{nm} B_{nm} J_o (\gamma_n \frac{r}{a}) \sin \frac{m\pi z}{h}.$$

The arbitary constants $B_{nm}$ can be found if simplifying assumptions are made about K, the electron production term. Consider the case in which the electron beam is suddenly switched into the cavity so that for $t < 0$, $K=0$, and for $t \gtrsim 0$, K is a constant, independent of time and geometry. This closely approximates the situation in the transient experiments reported in Section III. Then at $t = 0$, $n = K$, and for all times equation (6) must hold These considerations lead to the complete solution. With the definition $A_{nm} + B_{nm} = C_{nm}$, then

$$(7) \quad N = \sum_n \sum_m C_{nm} (1 - \frac{1}{\beta_{nm}}) J_o (\gamma_n \frac{r}{a}) \sin \frac{m\pi z}{h} e^{-\beta_{nm} t}$$
$$+ \sum_n \sum_m \frac{C_{nm}}{\beta_{nm}} J_o (\gamma_n \frac{r}{a}) \sin \frac{m\pi z}{h}$$

where

$$
(8) \quad
\begin{cases}
C_{nm} = \dfrac{8K}{m\pi\gamma_n J_1(\gamma_n)} & \text{for m odd,} \\[3mm]
C_{nm} = 0 & \text{for m even.}
\end{cases}
$$

From the First Quarterly Report, pages 25-27, an expression for the frequency shift of the cavity may be obtained:

$$
(9) \quad \Delta f = \frac{0.1 \displaystyle\int_v nE^2 d\tau}{1+(.055p)^2 \displaystyle\int_v E^2 d\tau}
$$

For the $TE_{011}$ mode of the rf cavity, $E \sim J_1(3.832\frac{r}{a})\sin\frac{\pi z}{h}$. Therefore equations (7) through (9) can be combined to produce an integral equation which will give $\Delta f$ as a function of time at any given pressure. Hand computation of this problem is extremely laborious but some machine computation and some hand calculations have been made for special cases. Combining that computation with some approximations, Figures 8, 9 and 10 demonstrate the type of solutions that equations (7) through (9) produce in typical cases.

Since a great deal of data has been taken using the beryllium foil diffusor with a more or less peaked angular distribution of electrons in the incident beam, it is instructive to rederive equations (7) and (8) for the case K not constant. For simplicity let

$$
(10) \quad K = kJ_0(\gamma_1 \frac{r}{a}), \quad \text{where K is a constant}
$$
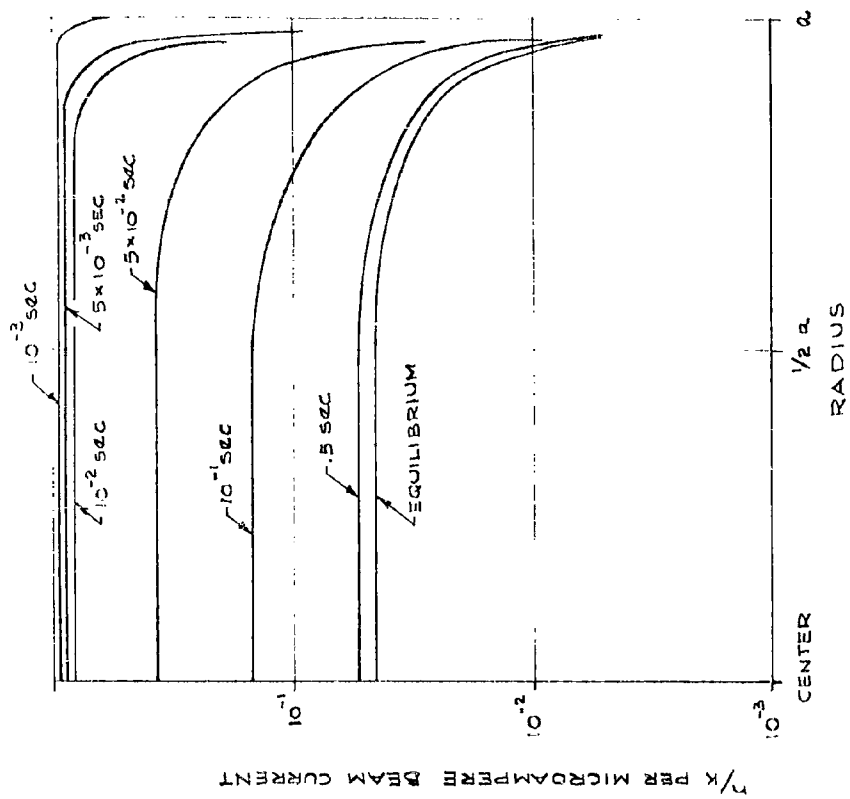
FIGURE 8
EVOLUTION OF RADIAL DISTRIBUTION OF
ELECTRON DENSITY FOLLOWING BEAM TURN-ON
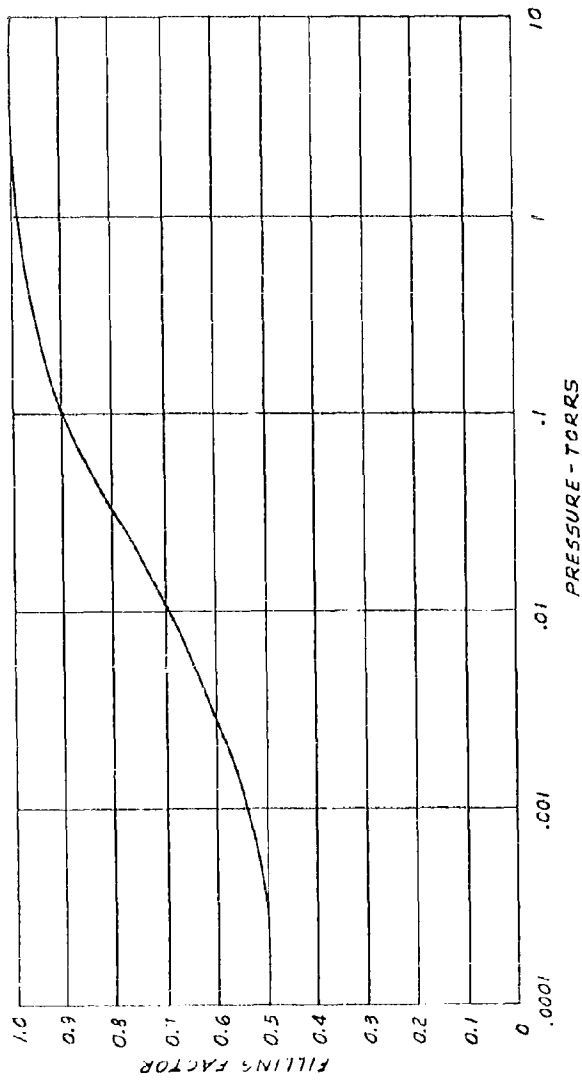
FIGURE 9

CALCULATED "FILLING FACTOR" $\int \frac{n}{n_o} E^2 dv / \int E^2 dv$ FOR OXYGEN

24
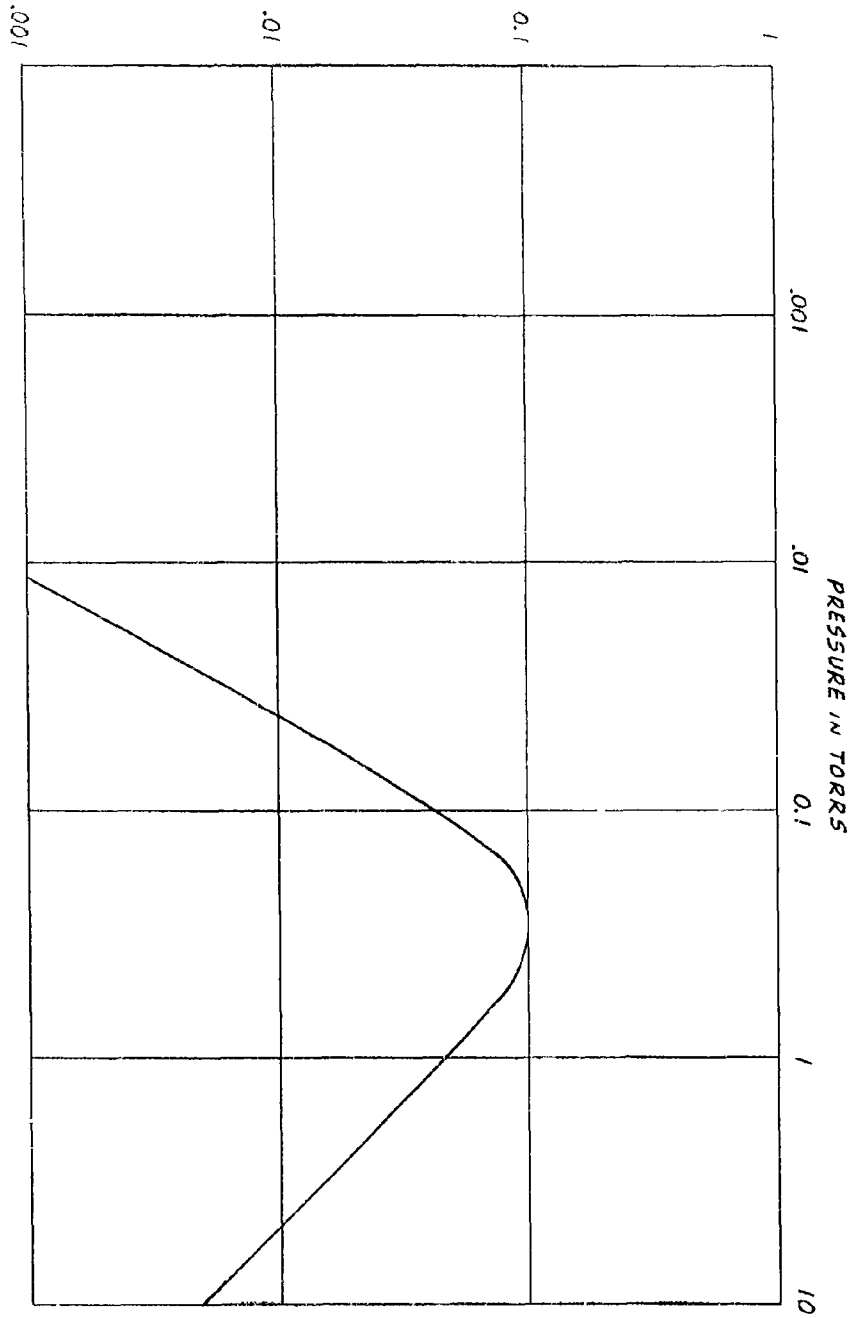


FIGURE 10
EQUILIBRIUM IONIZATION VERSUS PRESSURE
COMPUTED FROM EQUATION 7

Then at $t = 0$,

$$(11) \quad K = \sum_n \sum_m C_{nm} \, J_o \, (\gamma_{n}\frac{r}{a}) \sin \frac{m\pi z}{h} = k J_o(\gamma_{1}\frac{r}{a})$$

which has a solution for $C_{nm}$ as follows:

$$(12) \quad \begin{cases} C_{nm} = 0 \text{ for } n \neq 1 \text{ or } m \text{ even}, \\[2mm] C_{1m} = \dfrac{4k}{m\pi} \quad \text{for } n = 1 \text{ and } m \text{ odd.} \end{cases}$$

During the next quarter, numerical solutions for this as well as for other beam geometries, will be obtained, and compared with experiments.

## V.   AIR MEASUREMENTS

A very interesting phenomena was observed while doing transient
experiments in air.  The transient associated with diffusion occurred;
then, very slowly, "equilibrium" ionization density increased until a
plateau was reached, many minutes later, at a value of ionization
desnity two or three times larger than the initial density.

Figure 11 is a plot of typical time versus frequency shift
experiment in air showing the change in ionization with time.  It
took about nine minutes for the frequency to begin to shift per-
ceptibly, then the rise became quite steep, levelling off after
about 20 minutes.  The explanation for this phenomenon may possibly
be found in chemical reactions.  After reaching the high value of
ionization, if the Van de Graaff beam is shut off for 15 minutes
and then switched on again, the resulting ionization is at the high
level, not the initial low value.  In one case, after a two hour
wait with the beam off, the ionization at turn-on was 76% of the
previous peak value, and returned to that value in five minutes.
This behavior is suggestive of a reversible chemical reaction which
is driven by the electron beam in one direction but which slowly
reverses when the beam is off the cavity.

Figure 12 is a summary of all the air data taken to this date.
From Figure 12 it can be seen that the initial equilibrium ion-
ization is higher than in oxygen, as would be expected, but not as
high as would be predicted on the basis of published values for the
efficiency of nitrogen as the third body in electron attachment to
oxygen.  In fact, on Figure 12, the experiment marked "December 19"
at 0.5 Torr, has an initial slope of 2.5, very close to that of pure
oxygen (2.2) and rises up to 13, about five times higher.  The higher
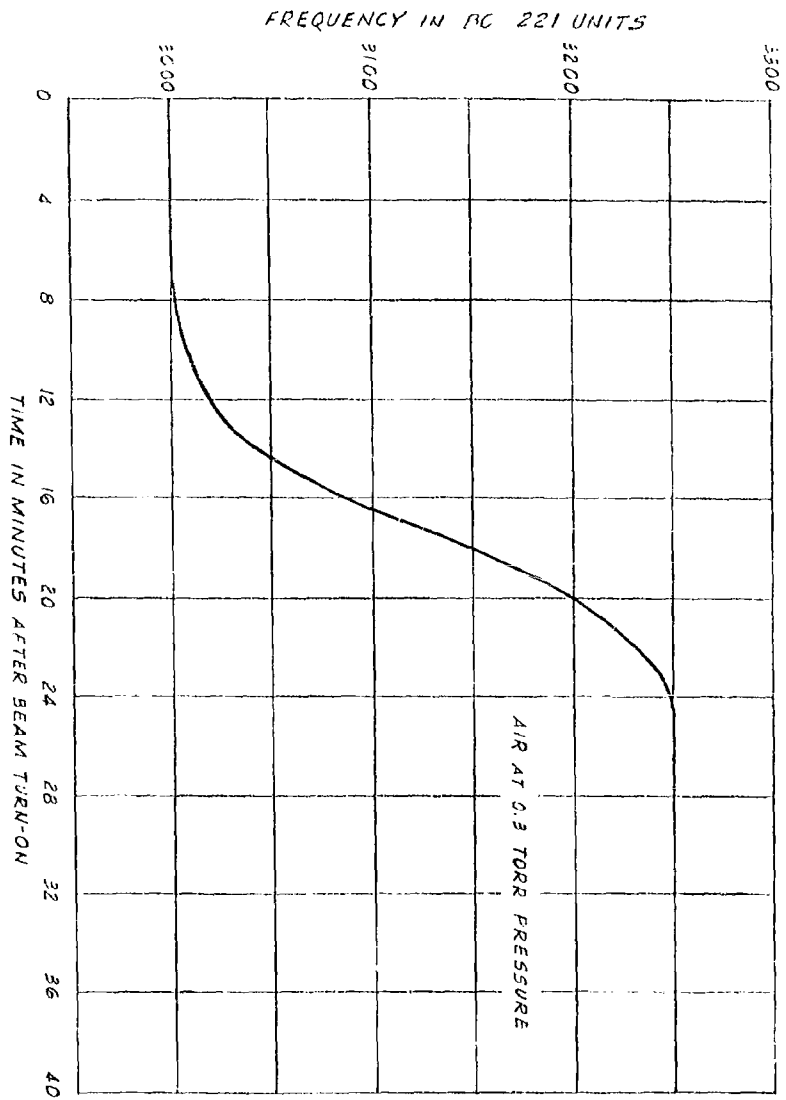
FIGURE 11
SLOW IONIZATION BUILD UP IN AIR
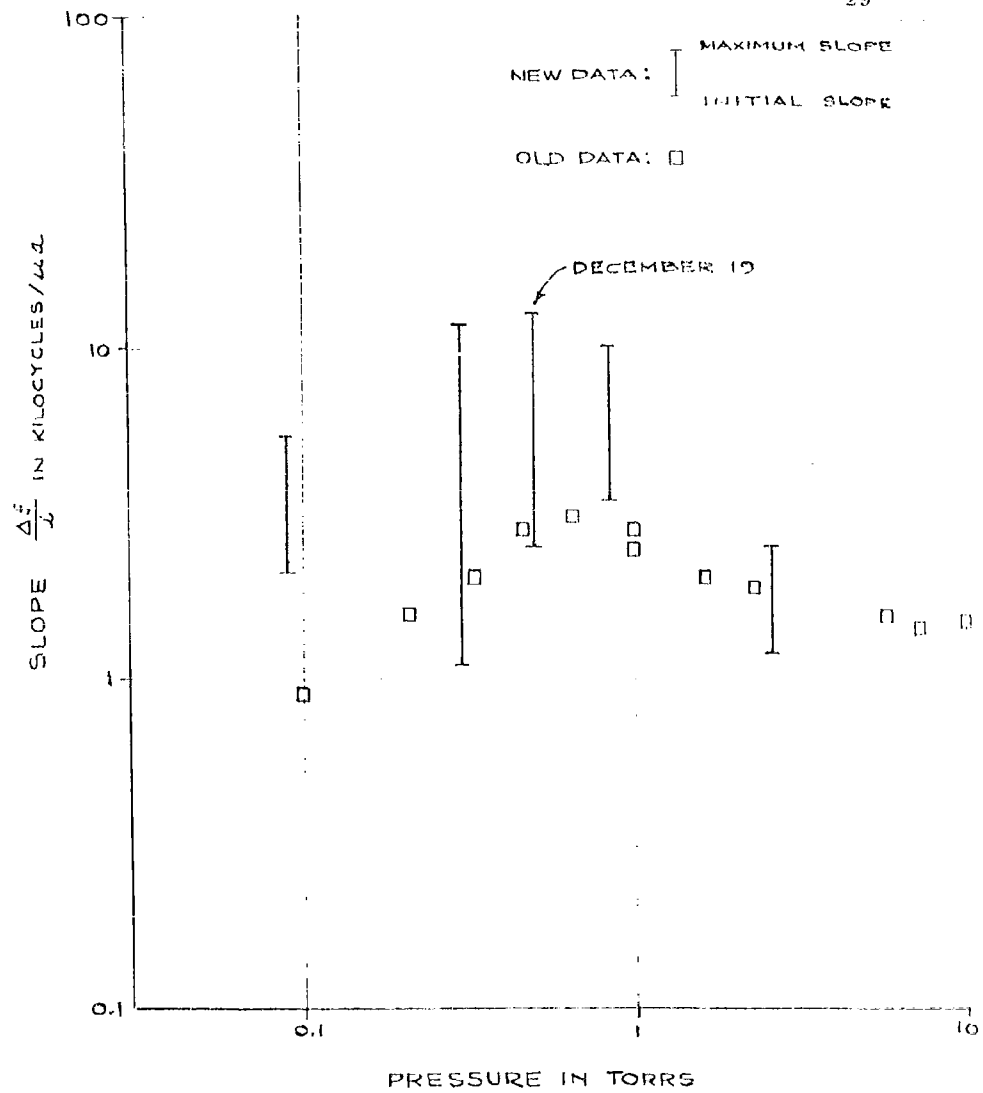
FIGURE 12
SUMMARY OF AIR DATA

values are more nearly indicative of what should be expected in air on the basis of its 20% oxygen content.

This phenomenon will be studied in more detail in the next quarter. In particular various $N_2 - O_2$ concentration ratios will be studied to unravel the chemistry.

## VI. PLANS FOR NEXT QUARTER

During the next quarter, enough data should be accumulated in oxygen to permit a complete analysis of the linear loss processes (that is, attachment and diffusion) in the regime of operating conditions employed in this work. Measurements in nitrogen and oxygen-nitrogen mixtures will be begun in detail, to determine the normal behavior of the mixtures and to search for radiation chemistry effects. The detailed calculation of the diffusion transient accompanying beam turn-on will be completed, and results compared with experiment.

In addition, a new dimension will be added to the measurement program during the quarter. An rf mass spectrometer will be designed and built, and probably attached to the cavity within the period. The spectrometer will be capable of observation of both positive and negative ions produced in the cavity. The addition of an internal ionizer, to permit studies of neutral molecules, has been delayed until the spectrometer itself is operative.

## VI. DISTRIBUTION LIST

OASD (R&E), Rm 3E1065
Attn: Technical Library
The Pentagon
Washington 25, D. C.     (1)

Chief of Research and
    Development
OCS, Department of the Army
Washington 25, D. C.     (1)

Chief Signal Officer
Attn: SIGRD
Department of the Army
Washington 25, D. C.     (1)

Chief Signal Officer
Attn: SIGOP-5
Department of the Army
Washington 25, D. C.     (1)

Chief Signal Officer
Attn: SIGAC
Department of the Army
Washington 25, D. C.     (1)

Chief Signal Officer
Attn: SIGPL
Department of the Army
Washington 25, D. C.     (1)

Director, U.S. Naval
    Research Laboratory
Attn: Code 2027
Washington 25, D. C.     (1)

Commanding Officer &
    Director
U. S. Navy Electronics
    Laboratory
San Diego 2, California (1)

U.S. National Bureau of
    Standards
Boulder Laboratories
Attn: Library
Boulder, Colorado     (1)

Commander
Aeronautical Systems Division
Wright-Patterson Air Force
Base, Ohio     (1)

Deputy President
U.S. Army Security Agency Board
Arlington Hall Station
Arlington 12, Virginia     (1)

Dr. K. S. W. Champion, CRZA
AFCRL, L. G. Hanscom
    Field
Bedford, Massachusetts     (1)

Dr. A. V. Phelps
Westinghouse Research Labs.
Beulah Road, Churchill Boro
Pittsburgh, Pennsylvania     (1)

Commanding Officer
U.S. Army Signal R&D Laboratory
Attn: SIGRA/SL-SA FU Mr. 1
Fort Monmouth, New Jersey     (1)

Commanding Officer
U.S. Army Signal R&D Laboratory
Attn: SIGRA/SL-DR
Fort Monmouth, New Jersey     (1)

U.S. Continental Army Command
    Liaison Office
U.S. Army Signal R&D Laboratory
Fort Monmouth, New Jersey     (3)

Air Force Command & Control
    Development Division
Attn: CCRR & CCSD
L.G. Hanscom Field
Bedford, Massachusetts     (2)

Commander, Rome Air Development
    Center
Attn: RAALD
Griffiss Air Force Base, New
    York     (1)

Air Force Cambridge Research
  Laboratories
Attn:  Research Library,
         CRXL-R
Laurence G. Hanscom Field
Bedford, Massachusetts  (1)

Chief, U.S. Army Security Agency
Arlington Hall Station
Arlington 12, Virginia  (2)

Corps of Engineers Liaison Office
U.S. Army Signal R&D Laboratory
Fort Monmouth, New Jersey  (1)

Commanding Officer
U.S. Army Signal Material
  Support Agency
Attn:  SIGMS-ADJ
Fort Monmouth, New Jersey  (1)

Commanding Officer
Diamond Ordnance Fuze Labs.
Attn:  Library, Rm. 211, Bldg. 92
Washington 25, D. C.     (1)

Dr. F. Byrne
Office of Naval Research
Washington 25, D. C.     (1)

Professor M. A. Biondi
Department of Physics
University of Pittsburgh
Pittsburgh 13, Pennsylvania (1)

Capt. James V. Lewis, Jr.
United States Air Force
AFSC Scientific and
  Technical Liaison Office
111 East 16th Street
New York 3, New York     (1)

Commander
Air Force Command and Control
  Development Division
Attn:  CRZC
L. G. Hanscom Field
Bedford, Massachusetts        (1)

Marine Corps Liaison Office
U.S. Army Signal R&D Laboratory
Fort Monmouth, New Jersey    (1)

AFSC Liaison Office
Naval Air R&D Activities Command
Johnsville, Pennsylvania      (1)

Commanding General
U.S. Army Electronic Proving
  Ground
Attn:  Technical Library
Fort Huachuca, Arizona        (1)

Commanding Officer
U.S. Army Signal R&D Laboratory
Attn:  Logistics Division
Fort Monmouth, New Jersey
M/F  SIGRA/SL-SAT-P. Brown/
W. Mc Afee                    (4)

Dr. William H. Kasner
Westinghouse Electric Corp.
Central Laboratories
Pittsburgh 35, Pennsylvania (1)

Professor Donald E. Kerr
Department of Physics
The Johns Hopkins University
Baltimore 18, Maryland        (1)